Breathing coherent phonons and caps fragmentation in carbon nanotubes following ultrafast laser pulses

Traian Dumitrică,[1] Martin E. Garcia,[2] Harald O. Jeschke,[3] and Boris I. Yakobson[4]

[1]*Department of Mechanical Engineering, University of Minnesota, Minneapolis, Minnesota 55455, USA*

[2]*Institut für Theoretische Physik, Universität Kassel, Heinrich-Plett-Str. 40, 34132 Kassel, Germany*

[3]*Institut für Theoretische Physik, Universität Frankfurt, Frankfurt, Germany*

[4]*Department of Mechanical Engineering and Materials Science, Rice University, Houston, Texas 77251, USA*

The response of carbon nanotubes to femtosecond laser pulses is studied with a nonadiabatic simulation technique, which accounts for the evolution of electronic and ionic degrees of freedom, and for the coupling with the external electromagnetic field. As a direct result of electronic excitation, three coherent breathing phonon modes are excited: two radial vibrations localized in the caps and cylindrical body, and one longitudinal vibration coupled to the nanotube length. Under high absorbed energies (but below 2.9 eV/atom, the graphite's ultrafast fragmentation threshold), the resulting oscillatory motion leads to the opening of nanotube caps. Following the cap photofragmentation the nanotube body remains intact for the rest of the 2 ps simulation time.

One of the most promising phenomena for controlling the properties of matter at the microscopic level is the in-phase collective motion of atoms driven by ultrafast laser pulses.[1–3] The necessary conditions for generating such *coherent* phonons are (i) the presence of Raman-active modes with inverse frequencies larger than a laser-pulse duration and (ii) the slow recombination dynamics of photoexcited carrriers. In carbon nanotubes (CNTs) (rolled graphene sheets with nanometer-size diameters), both conditions appear to be fulfilled: (i) Experiments on HIPCO samples, containing typically CNTs 1 nm in diameter, detected radial breathing mode (RBM) vibrations with a 133 fs period. (This period is larger than the duration of currently available ultrafast pulses.) (ii) Measurements[4–7] determined relatively long electron-phonon relaxation times in CNTs on the order of picoseconds. Conclusively, recent pump-probe experiments detected coherent RBM oscillations in response to 30 fs and sub-10 fs laser pulses.[6]

The apparent long lifetime of the electronic excitations implies that on subpicosecond time scales *nonthermal* effects will dominate the initial stages of a CNT's response. For the purpose of the simulation it is adequate to adopt a simplified physical picture:[8–10] The electronic subsystem (of initial temperature T_0) absorbs the optical energy and evolves towards a new equilibrium Fermi-type electronic distribution of temperature $T_e \gg T_0$. Meanwhile, in response to the softening of interatomic potentials, the ionic subsystem (also of initial temperature T_0) coherently departs from the equilibrium ground state, arrives at a new equilibrium, and oscillates around it with a new temperature $T_{ion} \ll T_e$. For longer times this metastable ephemeral state will be eliminated through electron-lattice equilibration.

Performing extensive molecular dynamics (MD) simulations based on the above physical model coupled with a tight-binding (TB) description of carbon,[11] we provide a microscopic picture of the femtosecond-scale response of capped CNTs to laser pulses. Selected results on nonthermal cap *release* and thermal fragmentation of (10,0) CNTs were

previously presented.[10] Here we show that the resulting CNT dynamics is essentially contained in three coherent breathing modes. Under higher excitations we identify two cap-opening mechanisms—*release* and *fragmentation*. Both mechanisms can be fully understood in terms of the induced coherent-phonon motion. The cap-opening process is demonstrated in (10,0), (5,5), and (8,4) CNTs.

Before turning to the simulation results we review the main ingredients of our MD method. We employ a mixed quantum-classical technique, which accounts for the quantum evolution and coupling to the external laser field of the electronic system, and for the classical motion of the ionic cores. The nonequilibrium dynamics of the N_e valence electrons is described by the equation of motion for the diagonal elements ρ_{ll} of the density matrix, written as

$$\frac{\partial \rho_{ll}}{\partial t} = \left.\frac{\partial \rho_{ll}}{\partial t}\right|_{coher} + \left.\frac{\partial \rho_{ll}}{\partial t}\right|_{coll}, \quad l = 1, N_e. \tag{1}$$

The first term in Eq. (1) represents the coherent contribution and contains the coupling of the electronic states to an external (classical) time-dependent field $E(\omega, t)$ of frequency ω. In the eigenstate basis of the unperturbed TB Hamiltonian H_{TB} (describing the electronic system), this term writes

$$\left.\frac{\partial \rho_{ll}(t)}{\partial t}\right|_{coher} = \frac{2}{\hbar^2} \text{Re}\left\{ \sum_m |x_{lm}|^2 E(\omega, t) e^{it\omega_{ml}} \int_{t-\Delta t}^t dt' E(\omega, t') \right.$$
$$\left. \times e^{it'\omega_{lm}} [\rho_{mm}(t') - \rho_{ll}(t')] \right\}. \tag{2}$$

x_{lm} represents the dipole-matrix element between the TB states $\hbar\omega_{lm} = \epsilon_l - \epsilon_m$, with ϵ_l being the eigenvalues of H_{TB} and Δt is the integration time step of 0.1 fs. Invoking the rotating-wave approximation, Eq. (2) can be transformed into a more computationally suitable form.[8]

The second term in Eq. (1) is the Coulomb collision rate, treated phenomenologically as

$$\partial \rho_{ll} / \partial t |_{coll} \simeq - [n_l(t) - n_l(\mu, T_e)] / \tau_{e\text{-}e}. \qquad (3)$$

It transforms the nonequilibrium electronic distribution $n_l(t)$ created under the influence of an external electromagnetic (e.m.) field into a Fermi-type function $n_l(\mu, T_e)$ within the relaxation time $\tau_{e\text{-}e}$. T_e and μ are the electronic temperature and chemical potential, respectively. They are obtained from the amount of absorbed energy E_{abs} at time t, $E_{abs}(t) = E(t) - E(0)$, by imposing that N_e remains constant.

To perform MD simulations the force $\mathbf{F_X}$ acting on the ion at position $\mathbf{X}$ is needed. For this we move to a thermodynamic formulation: When the N_e electrons are in equilibrium at T_e, the free energy thermodynamic potential $U = E - T_e S - \mu N_e$ is minimized. Here $S = -k_B \Sigma_l [n_l \ln n_l + (1-n_l) \ln(1-n_l)]$ is the entropy function. By differentiating the energy, $dE = T_e dS + \mu dN - \Sigma_\mathbf{X} \mathbf{F_X} d\mathbf{X}$, one gets $dU = -S dT_e + N_e d\mu - \Sigma_\mathbf{X} \mathbf{F_X} d\mathbf{X}$. Thus, in thermodynamic form, $\mathbf{F_X} = -(\nabla_\mathbf{X} U)_{T_e, \mu}$. Introducing the electronic energy and the equilibrium Fermi-Dirac electronic distribution $n_l = 1/\{1 + \exp[(\epsilon_l - \mu)]/k_B T_e\}$ into U, one obtains the electronic part of the force as

$$\mathbf{F_X} = - \sum_{l,l'} \rho_{ll'} \nabla_\mathbf{X} H_{ll'}^{TB}, \qquad (4)$$

which is the Hellmann-Feynman theorem. Following the laser pulse and equilibration of the electronic system at T_e, the thermodynamic forces (4) are leading the system to the new metastable equilibrium. Computationally, the ionic system is evolved in time with a symplectic velocity Verlet scheme, using a time step of 0.1 fs.

We note that our approach involves several approximations. (i) The classical description of ionic motion, attained by averaging over the electronic quantum states [as indicated in Eq. (4)], is inadequate for studying quantum behaviors such as squeezed coherent phonons[12] or branching phenomena, for which surface-hopping methods[13] are appropriate. Since here we are interested in the soft-acoustic-phonon modes, a classical description is justified. (ii) The employed one-electron picture does not include excitonic corrections. Although excitons play a central role in CNT optical-absorption experiments,[14] they appear less relevant in the subsequent structural dynamics.[15] (iii) Throughout simulations we use TB parameters without performing self-consistent cycles. It can be shown[16] that for fixed T and μ, U is stationary with respect to $n_l \rightarrow n_l + dn_l$ and norm-conserving $\phi_l(\mathbf{x}) \rightarrow \phi_l(\mathbf{x}) + \delta\phi_l(\mathbf{x})$ one-electron eigenfunction variations. Thus, the TB guess appears as second-order in dn.

In the simulations presented next we relate the strength of the laser pulse indirectly with the amount of optical absorbed energy E_{abs}. The most common measure of the pulse intensity is the fluence F, defined as the total energy per unit area carried over the duration of the pulse. Considering the data for graphite, i.e., $r = 30\%$ reflectivity of the laser pulse at the sample surface, $d = 32$ nm laser-penetration depth, and atom concentration $\rho = 1.14 \times 10^{23}$ atoms/cm³, we equate $\rho d E_{abs} = (1-r)F$. It follows that $E_{abs} = 1$ eV/atom corresponds to $F = 0.085$ J/cm². Due to the lack of similar data, we will use graphite to estimate F in CNTs.

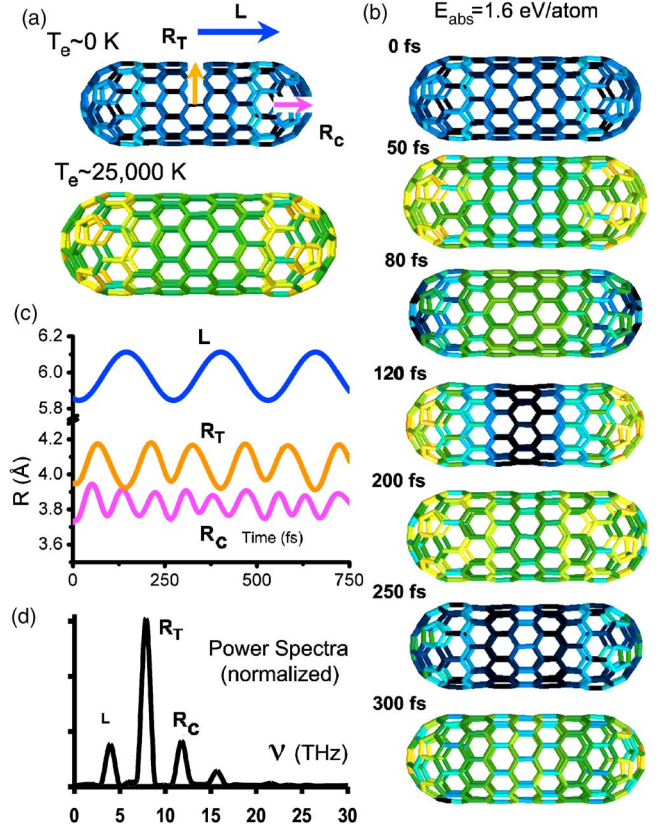

FIG. 1. (Color online) (a) Optimized geometries of a (10,0) capped CNT under electronic temperatures of 0 K and 25 000 K. Arrows mark the spherical (R_C) and cylindrical (R_T) radii, and the tubular half length (L). The C-C bonds lengths vary from 1.4 Å shown in blue (dark gray) to 1.52 Å shown in yellow (light gray). Response following absorption of 1.6 eV/atom from a 10 fs laser pulse of 1.9 eV photon energy: (b) Time evolution of the geometry during the first 300 fs. (c) R_C, R_T, and L, for the first 750 fs. (d) Vibrational power spectrum.

To understand the lattice response to laser pulses we first address the effect of high electronic excitation on the CNT's shape. Exploiting the flexibility of our MD method, we performed simulated annealing toward a 0 K lattice temperature while *maintaining* a very high T_e.

Figure 1(a) depicts the configurations obtained following a careful annealing of a (10,0) capped CNT containing 200 atoms, with $T_e \sim 0$ K. The bond-length information is carried by a color (gray) code of blue (dark gray) at $l_{C\text{-}C} \lesssim 1.4$ Å, ranging to yellow (light gray) at $l_{C\text{-}C} \gtrsim 1.52$ Å. An interesting magnitude associated with $l_{C\text{-}C}$ is the local strain. It is not surprising to find that the most strained bonds are at the caps, where curvature is greatest. Next, T_e was raised to 25 000 K. By inspecting the new CNT configurations it is visible that this dramatic T_e increase produces a significant C-C bond expansion (or weakening). To characterize the resulting shape change we compared the tubular half length L and radius R_T, and the average hemispherical cap radius R_C. A 3% overall increase in L, R_T, and R_C was measured.

Now we focus on the dynamical response. We begin by describing results obtained under low E_{abs}, when the CNT remained intact during the 2 ps simulation time. The goal is
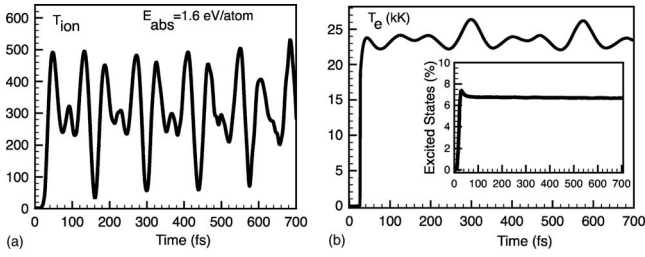
FIG. 2. Time dependence of the (a) ionic T_{ion} and (b) electronic T_e temperatures following absorption of 1.6 eV/atom ($F = 0.14$ J/cm^2). The insert shows the occupancy of excited states.

to identify the phonons excited by the noted volumetric change.

Figures 1(b)–1(d) summarize the (10,0) CNT response following the absorption of a 1.6 eV/atom from a 10 fs laser pulse of 1.9 eV central photon energy. The immediate ion dynamics transpires from the time sequence of geometries shown in Fig. 1(b). The colored (gray) bonds unveil the impulsively excited vibrational modes, showing a distinct *spatial* coherence in the cap and tube areas.

The *temporal* coherence can be followed in Fig. 1(c), which monitors the evolution of R_C,[17] R_T, and L. Following the optical absorption (at $t=0$ fs), the caps and the tube start expanding in phase but, due to the different intrinsic oscillation frequencies, the maxima and minima are reached at different times. At ~ 130 fs the caps' radial expansion and tubule maximum elongation coincide with the tubule radial contraction and, after another ~ 130 fs the initial CNT shape is reached.

The correlation encountered in the 0–260 fs time interval is maintained for the rest of the simulation. Obtained temporal periodicity with little damping (dephasing) calls for the analytical approximations (in Å)

$$R_C(t) = 3.83 - 0.06 \cos(6\pi t/257 \text{ fs}), \quad (5a)$$

$$R_T(t) = 4.05 - 0.10 \cos(4\pi t/260 \text{ fs}), \quad (5b)$$

$$L(t) = 5.98 - 0.12 \cos(2\pi t/257 \text{ fs}). \quad (5c)$$

The power spectrum of Fig. 1(d) was obtained by taking the Fourier transform of the velocity autocorrelation function over an interval of 1 ps following the completion of the laser pulse. Interestingly, the most noticeable features can be unambiguously assigned based on Eqs. (5): There are two coherent RBM excitations, localized in the cap ($\nu_C^{RBM} = 11.6$ THz) and nanotube body ($\nu_T^{RBM} = 7.7$ THz), and a soft longitudinal excitation ($\nu_L = 3.9$ THz) that couples with the tubular CNT length.

The instantaneous value of the ionic temperature T_{ion} is shown in Fig. 2(a). The initial T_{ion} increase is followed by large oscillations around the mean value of ~ 300 K. These high-amplitude fluctuations confirm that equilibration was not reached as the lattice vibration is mainly contained in three phonon modes. By contrast, the irradiated electronic system reaches extremely high temperatures, as indicated in
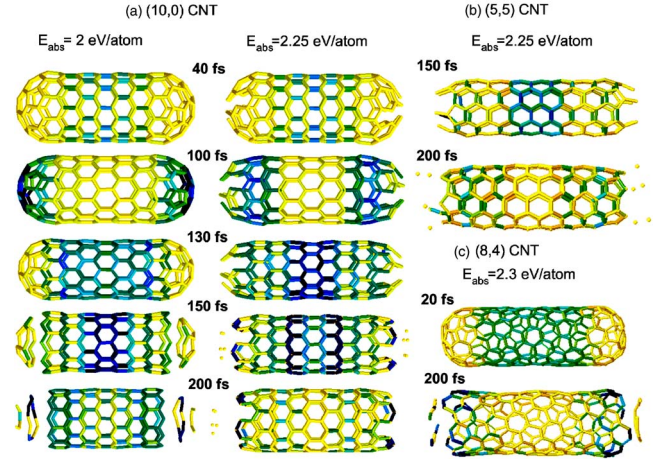

FIG. 3. (Color online) Cap opening mechanisms in (a) (10,0) CNTs: cap release (left) and partial cap fragmentation (right), (b) (5,5) CNT: partial cap fragmentation, and (c) (8,4) CNT: total cap fragmentation. The color (gray scale) code is the same as in Fig. 1.

Fig. 2(b). The insert shows the occupancy of antibonding states expressed as a percentage of the total number of valence electrons.

Notably, the longitudinal mode cannot be properly described if the usual periodical boundary conditions are imposed over the CNT body. A useful analytical description for this mode can be obtained from a continuum analysis, i.e., by solving the wave equation for a nanotube of length $2L$ under stress-free boundaries, i.e., $(\partial u/\partial z)|_{z=-L,L}=0$. The displacement field u at position z along the CNT axis writes

$$u(z,t) = A \sin(\pi z/2L)\cos(c\pi t/2L), \quad (6)$$

where amplitude A depends on E_{abs} and L, and c represents the speed of sound. Fitting to the data of Fig. 1(c) gives $A = -0.12$ Å and $c = 9\,307$ m/s.

Next we focus on the responses under higher E_{abs}, aiming for structural changes. Figure 3 displays representative snapshots showing that the tubular part remains structurally stable but the caps open. We interpret these results in terms of the coherent phonon motion.

Figure 3(a) displays two simulations for the response of a (10,0) CNT. Following the absorption of a 2.0 eV/atom, an immediate elongation of the bonds situated in the caps occurred. Due to the still strong bonding, caps survive this initial displacive expansion. However, the next 100 fs brings an *out-of-phase* cap-tube RBM oscillation sequence, which subjects the cap-tube interface to an increased strain. After 130 fs an additional strain is caused by the longitudinal mode, which starts to retract. The *release* of the caps follows at ~ 150 fs. Under 2.25 eV/atom irradiation, caps cannot sustain the initial impulsive RBM. The weaker pentagonal rings are partially or totally breaking (function of location) after only 40 fs of exited-state dynamics, when the cap-tube RBM oscillations are still *in-phase*. Following the emission of 5 atoms per cap (after ~ 150 fs) the spherical curvature is completely destabilized. The remaining caps' atoms tend to move back toward one another but no bond reformation was observed. Figure 3(b) shows that under the same E_{abs}

=2.25 eV/atom value, the fragmentation mechanism is essentially reproduced in a (5,5) CNT composed of 180 atoms.

During the initial in-phase oscillation sequence and under still higher E_{abs} values, we obtained that the entire caps fragment due to a more vigorous RBM excitation combined with a weaker C-C bonding. Two representative snapshots from a simulation involving an (8,4) CNT containing 260 atoms under E_{abs}=2.3 eV/atom are shown in Fig. 3(c). The emission of whole caps containing 14 atoms each is observed after ~200 fs following irradiation. During the next 1 200 fs the nanotube body remained structurally stable.

Above the 2.8 eV/atom absorption value, simulations show that the tube body fragments. It is useful to know that the experimental ultrafast optical damage threshold[18] in the graphene layer occurs at F_{th}=0.25 J/cm^2 or E_{abs}~2.9 eV/atom. The nonthermal cap opening reported here was obtained under laser fluences below F_{th}. Interestingly, well above this value, under F=7.5 J/cm^2 onionlike structures and multiwall CNTs were experimentally obtained[19] from graphite.

We have performed MD simulations that provide a detailed microscopical understanding of the zero-state response of capped nanotubes to ultrafast laser pulses. We emphasize that in contrast to conventional ground-state simulations, the employed method accounts for the population of each one-electron state during the ion motion. As can be seen from Fig. 1, the lattice vibration following ultrafast light absorption couples strongly with the cylindrical (body) and spherical (caps) CNT's shape. Our main result is presented in Fig. 3. It is shown that for E_{abs} values situated below graphene's ultrafast ablation threshold, a selective cap fragmentation occurs. This process can be fully understood based on the dynamics generated by the laser-induced coherent phonons, which are analyzed in Figs. 1 and 2.

To address the whole catalog of the CNT species, we recall that a tube is characterized by its radius R_T and wrapping angle χ. Since optical absorption is dependent on these parameters,[20,21] to excite coherent phonon motion in general, the laser pump photon energy will need to be adjusted. The precise E_{abs} values to produce photofragmentation should have a weak R_T dependence. Next, invoking the CNT isotropic elastic properties, it is clear that once excited, the breathing coherent phonons will scale with R_T and L, but will not with χ. For this reason the coherent dynamics observed for (10,0) CNTs holds for the (5,5) and (8,4) equal-curvature CNTs, leading to their cap opening in Figs. 3(b) and 3(c), respectively.

Concerning the curvature dependence, we note that the RBM period increases with R_T. Our estimate based on experimental data[20] indicates that only at very large radii the RBM period becomes comparable with the electron-phonon relaxation time (for R_T~6 nm, $1/\nu_{RBM}$=1 ps). From an elastic-isotropic model it appears that both RBMs of a sphere and a cylinder scale with curvature.[22] It follows that for the same R_T, the RBM frequency fraction remains constant, $\omega_{\mathrm{sphere}}/\omega_{\mathrm{cylinder}}=2\sqrt{(\lambda+\mu)/(\lambda+2\mu)}$, where λ and μ are the Lamè material coefficients. Thus, we can conjuncture that the cap-tube RBM oscillation sequences of Fig. 1(c) and the cap-opening mechanisms will hold for any CNT.

Technologically, the opening of a CNT's caps is a challenging issue currently approached with chemical methods.[23] The microscopic simulations presented here suggest an interesting alternative, where cap opening occurs as a CNT responds to the "initial conditions" created by an ultrafast laser pulse.

[1] For a review, see e.g., T. Dekorsy, G. C. Cho, and H. Kurz, *Light Scattering in Solids VIII*, edited by M. Cardona and G. Gütherodt (Springer, Berlin, 2000).

[2] G. A. Garrett *et al.*, Phys. Rev. Lett. **77**, 3661 (1996); S. Hunsche *ibid.* **75**, 1815 (1995).

[3] M. Hase *et al.*, Phys. Rev. Lett. **88**, 067401 (2002).

[4] T. Hertel and G. Moos, Phys. Rev. Lett. **84**, 5002 (2000); J.-S. Lauret *et al.*, *ibid.* **90**, 057404 (2003).

[5] G. N. Ostojic *et al.*, Phys. Rev. Lett. **92**, 117402 (2004).

[6] C. Manzoni *et al.*, Phys. Rev. Lett. **94**, 207401 (2005); A. Gambetta *et al.*, Nat. Phys. **2**, 515 (2006).

[7] R. J. Ellingson *et al.*, Phys. Rev. B **71**, 115444 (2005).

[8] H. O. Jeschke, M. E. Garcia, and K. H. Bennemann, Phys. Rev. B **60**, R3701 (1999); H. O. Jeschke, M. E. Garcia, and K. H. Bennemann, Phys. Rev. Lett. **87**, 015003 (2001).

[9] T. Dumitrică and R. E. Allen, Phys. Rev. B **66**, 081202(R) (2002); T. Dumitrică and R. E. Allen, Laser Part. Beams **20**, 237 (2002); T. Dumitrică *et al.* Phys. Status Solidi B **241**, 2331 (2004).

[10] T. Dumitrică *et al.*, Phys. Rev. Lett. **92**, 117401 (2004); M. E. Garcia *et al.*, Appl. Phys. A **79**, 855 (2004).

[11] C. H. Xu *et al.*, J. Phys.: Condens. Matter **4**, 6047 (1992).

[12] O. V. Misochko, K. Sakai, and S. Nakashima, Phys. Rev. B **61**, 11225 (2000).

[13] J. C. Tully, J. Chem. Phys. **93**, 1061 (1990); C. F. Craig, W. R. Duncan, and O. V. Prezhdo, Phys. Rev. Lett. **95**, 163001 (2005).

[14] F. Wang *et al.*, Science **308**, 838 (2005); Y.-Z. Ma *et al.*, Phys. Rev. Lett. **94**, 157402 (2005).

[15] M. Zamkov *et al.*, Phys. Rev. Lett. **94**, 056803 (2005); B. F. Habenicht, C. F. Craig, and O. V. Prezhdo, *ibid.* **96**, 187401 (2006).

[16] T. N. Todorov, J. Hoekstra, and A. P. Sutton, Philos. Mag. B **80**, 421 (2000).

[17] The $R_C(t)$ measurement is less trivial due to the longitudinal motion. From the radius measured from a static caps center,[10] here we filtered out the Fourier component associated with the longitudinal mode L shown in Fig. 1(c).

[18] K. Sokolowski-Tinten *et al.*, in *Ultrafast Phenomena XI*, edited by T. Elsaesser *et al.*, Springer Series in Chemical Physics Vol. 66 (Springer, Berlin, 2000), p. 425.

[19] S. Eliezer *et al.*, Laser Part. Beams **23**, 15 (2005).

[20] S. M. Bachilo *et al.*, Science **298**, 2361 (2002).

[21] V. N. Popov and L. Henrard, Phys. Rev. B **70**, 115407 (2004).

[22] S. Erdin and V. L. Pokrovsky, Int. J. Mod. Phys. B **15**, 3099 (2001).

[23] P. M. Ajayan *et al.*, Nature (London) **362**, 522 (1993).